How to cite: *Angew. Chem. Int. Ed.* **2021**, *60*, 7316–7322
International Edition: doi.org/10.1002/anie.202014329
German Edition: doi.org/10.1002/ange.202014329

Analytical Methods

Enhancing the Sensitivity of Photoelectrochemical DNA Biosensing Using Plasmonic DNA Barcodes and Differential Signal Readout

*Amanda Victorious[+], Sudip Saha[+], Richa Pandey, and Leyla Soleymani**

Abstract: *Photoelectrochemical biosensors hold great promise for sensitive bioanalysis; however, similar to their electrochemical analogues, they are highly affected by the variable backgrounds caused by biological matrices. We developed a new PEC biosensing strategy that uses differential signal generation, combining signals from two separate but correlated binding events on the biosensor, for improving the limit-of-detection, sensitivity, and specificity of PEC DNA biosensors in biological samples. In this assay, the binding of unlabeled target DNA is followed by the capture of a signal amplification barcode featuring a plasmonic nanoparticle. The interaction of the plasmonic barcode with the semiconductive building blocks of the biosensor results in significant signal amplification, and together with differential signal processing enhances the limit of detection and sensitivity of the assay by up to 15- and three-fold, respectively, compared to the previously-used PEC assays with a single binding event, demonstrating a limit of detection of 3 fM.*

Introduction

Photoelectrochemical (PEC) biosensors have been heavily explored over the past decade due to their promise for improved signal-to-noise ratio and enhanced limit-of-detection.[1–3] These biosensors translate specific biorecognition events into a change in the output PEC signal.[1,4] As with their electrochemical analogues, the limit-of-detection of PEC transducers is often compromised due to signal fluctuations caused by environmental interferents and minute variations in experimental conditions.[5–7] In response, ratiometric or differential assays, combining two or more PEC signals, have been implemented to reduce the effect of interference and experimental variations, enhance detection accuracy at trace analyte concentrations, and improve analysis reliability.[8–10]

The existing ratiometric PEC biosensors typically use multiple photoactive species—signal reporters[9,11,12] or labels[8]—that need to be activated at various voltages[11,12] or wavelengths[8] in order to obtain multiple signal readings for each biorecognition event. Although this multi-species approach is effective in increasing the signal-to-noise ratio of PEC biosensors, it increases the complexity of the measurement instrumentation and the calibration algorithms needed to deal with the varying baseline signals and chemical and optical stability observed when multiple photoactive materials are used in a single system.

For PEC biosensors to be translated from the laboratory to the market, it is highly desirable for high sensitivity and specificity to be paralleled with facile operation and instrumentation. As a result, new approaches for ratiometric/differential PEC signal transduction using a single photoactive species, operated at a single voltage using a single light source are needed.

Several PEC biosensors have recently been developed that use the interaction between plasmonic nanoparticles (NPs) such as Au and Ag with semiconductive photoelectrodes to translate biomolecular recognition to a change in the PEC signal.[13,14] Among these, systems that use robust and stable materials are highly desired for use in biosensing devices that undergo multiple washing, incubation, and potential scan steps. Au/TiO_2 systems offer excellent chemical and photostability and have been used in protein,[15] heavy metal,[16] glucose[17] and nucleic acid detection.[18] The major role of Au NPs in these sensing systems is to improve the photoconversion efficiency of the functionalized TiO_2 electrodes upon biorecognition, thereby enhancing the photocurrent. Depending on the assay design, different roles—injection of hot charge carriers, extending the light absorption range, and excitation of charge carriers in TiO_2 via plasmon energy transfer—can be played by the Au NPs upon target binding to modulate the photocurrent.[19–21] More specifically, biorecognition causes the Au NPs to either come into proximity[22] of (*signal-on*) or move away[20] from (*signal-off*) the TiO_2 electrodes. However, these bioassays only focus on harnessing the modulation of photocurrent influenced by Au NPs.

In this work, we sought to answer the question: Is it possible to effectively utilize and combine photocurrent modulation—both upon the capture of the unlabeled target and the binding of a plasmonic barcode (Au NP-modified DNA strand)—to achieve improved analytical sensitivity?

We aimed at developing a differential biosensor using the TiO_2/Au system, using Au NPs as the sole PEC species. To achieve this, we investigated the use of two subsequent and correlated PEC measurements. First, we measured the change in PEC current induced by the binding of an unlabeled target to a probe DNA. Second, we measured the additional PEC current change obtained when the unreacted probes were

[*] A. Victorious,[+] S. Saha,[+] Prof. L. Soleymani
School of Biomedical Engineering, McMaster University
1280 Main Street West, Hamilton, Ontario, L8S 4L7 (Canada)
E-mail: soleyml@mcmaster.ca
R. Pandey, Prof. L. Soleymani
Department of Engineering Physics, McMaster University
1280 Main Street West, Hamilton, Ontario, L8S 4L7 (Canada)
[+] These authors contributed equally to this work.
Supporting information and the ORCID identification number(s) for the author(s) of this article can be found under: https://doi.org/10.1002/anie.202014329.

bound to a signal amplifying barcode (SAB) generated from AuNP-labeled DNA strands, for signal amplification. The signal changes measured during the two binding events were differentially combined to enhance the limit of detection (LOD) of the system. The use of SAB as an amplification sequence builds on the premise that plasmonic NPs in direct contact or close proximity to semiconducting materials possessing favorable energetics, modulate carrier lifetime,[23,24] thus, altering the PEC current. Using this differential strategy, the influence of background contributions is effectively suppressed, which in turn enhanced sensitivity by more than three times and LOD by 15 times compared to an analogous assay that measured a single binding event.

Results and Discussion

We created the differential PEC biosensor by combining two sequential but correlated binding events on a single photoelectrode. A porous network of TiO_2 NPs was deposited on ITO substrates to create the photoelectrode, yielding the initial photocurrent profile (Figure 1a, (i)). These photoelectrodes were then bio-functionalized with 15-nucleotide long single stranded DNA (ss-DNA) probes and subsequently blocked with monoethanolamine (MEA) to prevent non-specific adsorption. The immobilization of probe DNA on the photoelectrode surface was verified using chronocoulometry and the probe coverage was measured as 5×10^{11} molecules cm^{-2} (Supporting Figure S1).

A resulting decrease in photocurrent was anticipated following bio-functionalization due to the induction of steric hindrance between the photoelectrode and the species in the electrolyte (Figure 1a, (ii)). Upon incubation with 25-mer complementary DNA targets (unlabeled), hybridization occurs between a fraction of the total probe population and the targets, leaving behind a population of available unhybridized probe strands. A further decrease in photocurrent is expected due to steric hindrance (Figure 1a, (iii)). The SAB strand is then hybridized with the available probe strands. The length of the ssDNA probe (15-mer) is shorter than the length of the

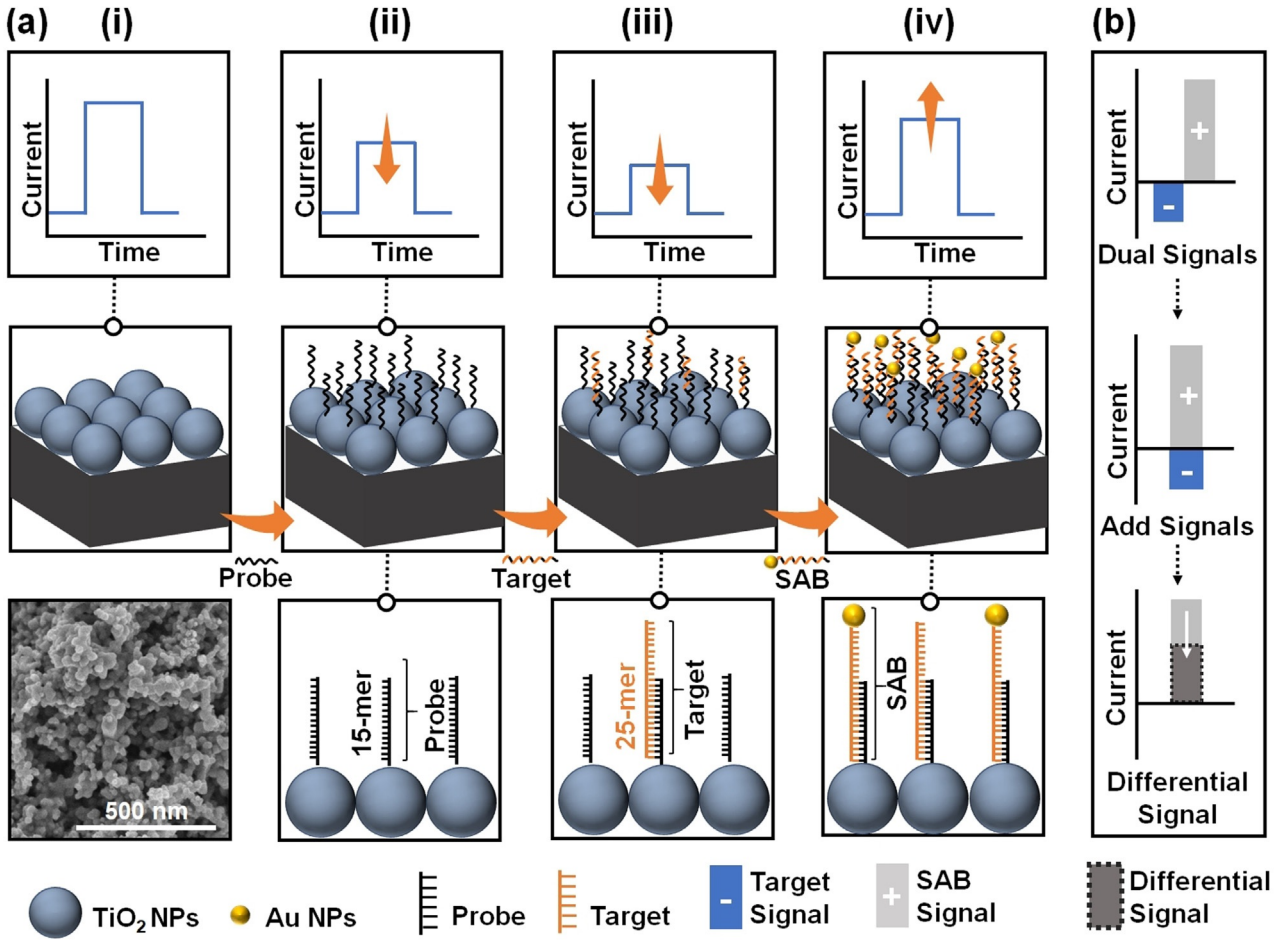

Figure 1. The operation of the differential PEC biosensor. a) Schematic illustration depicting the development of the PEC biosensor with the expected change in photocurrent profile depicted at each stage of sensing: (i) Baseline photoelectrodes are created via solution deposition of TiO_2 NPs onto ITO substrates, yielding an anodic photocurrent upon 405 nm illumination. (ii) Bio-functionalized photoelectrodes are created by depositing 15-mer DNA probes on photoactive TiO_2 substrates, yielding a decrease in photocurrent. (iii) 25-mer nucleotide targets are hybridized onto the transducer, resulting in a further decrease in photocurrent. (iv) Introducing SABs gives rise to an amplified photocurrent following hybridization. An SEM image demonstrates the photoelectrode surface structure (bottom left). b) A depiction of the combination of signals following target and SAB hybridization to yield the differential signal processing scheme used in this study.

SAB strand (25-mer), with the resulting DNA complex containing both double and single stranded regions.[25,26] It has been previously demonstrated that the Au NPs on the SAB have a high probability of coming into direct contact with TiO_2 NPs owing to the dynamic motion of the DNA complex used in this work.[18] Direct contact between Au and TiO_2 NPs facilitates charge transfer between the two particles, thereby enhancing the anodic photocurrent (Figure 1a, (iv)).[27,28] The presented DNA sensing approach, involving two hybridization steps, presents two benefits: 1) the target DNA strand does not need to be labeled prior to introduction on the chip, and 2) the combination of the signal changes induced from the two hybridization steps is expected to increase the assay sensitivity (Figure 1b). It should be noted that this two-hybridization approach makes it possible for the SAB binding to result in the displacement (completely or partially) of the target strands.[29,30] Partial hybridization of the SAB with the existing target-hybridized probes becomes more probable at longer nucleic acid strands.[29,31] Under the conditions used here, the use of a 15-mer DNA probe, a 25-mer DNA target, a 25-mer SAB strand with the same sequence as the target strand, and a room temperature hybridization step, we expect less than 10% of target strands to be removed by the SAB strand,[29,30] thus not making competitive strand replacement a significant contributor to the assay performance. As a result of the assay design, we expect it to be ideally-suited for detecting short nucleic acid targets such as microRNA (18–25 mer) or short DNA barcodes released from DNA machines.[32] MicroRNAs have been identified as clinically important diagnostic biomarkers for various diseases including cancer,[33,34] cardiovascular conditions,[35] and infectious diseases.[36]

The differential sensor design was verified by measuring the photocurrent and charge transfer resistance in each step of the sensor development process (Figure 2). For the photocurrent measurements, we used an LED light source with an excitation wavelength of 405 nm and an intensity of 160 $W m^{-2}$. Ascorbic acid (AA) was used as the hole scavenger to generate an anodic current upon optically exciting the electrode (Figure 2a). A 45% photocurrent decrease was observed after probe deposition due to the steric hindrance of AA caused by the single stranded capture probe (Figure 2b).[37] Subsequently, MEA was used to block the unbound sites of the working electrode which further decreased the photocurrent by 35% as MEA impedes the access of AA to the surface of TiO_2 nanoparticles. Following this, target DNA was introduced on the surface and a 45% photocurrent reduction was observed. As target DNA hybridizes with the capture probe on the photoelectrode, it further hinders the access of AA (Figure 2a). Finally, a 105% enhancement in photocurrent was observed upon the introduction of the SAB to the substrate (Figure 2b). Enhancement of photocurrent under UV excitation has been reported in similar systems due to Fermi level equilibration as optically-excited electrons from the conduction band of the semiconductor move to the Au NPs, thereby reducing the carrier recombination rate.[38,39] Optical excitation at 405 nm can also generate hot electron and hot holes via d-sp transition in Au NPs.[40–42] It is possible that these hot holes directly oxidize AA, while the hot electrons are transferred to TiO_2 NPs, thereby increasing the photocurrent (Figure 2a).

Electrochemical impedance spectroscopy (EIS) at open circuit potential was also used to characterize the stepwise fabrication process of the proposed assay design (Figure 2c). The charge transfer resistance (R_{ct}) of the photoelectrode decreased by 78% after DNA probe attachment (Supporting Table S1 and Supporting Figure S2). This is contrary to the usual observation found in the literature where probe immobilization increases R_{ct}.[43–45] A study reported by Imani et al. showed that the addition of ssDNA on dopamine modified TiO_2 NPs results in a higher electron transfer rate due to the quantum mechanical tunneling effect by bridging the molecular medium between the donor and the acceptor sites of ssDNA and TiO_2 NPs, respectively.[46] Therefore, the observed reduction in R_{ct} in this work can also occur due to the amine-modified ssDNA covalently bonding with the aldehyde groups on the 3,4-dihydroxybenzlaldehyde (DHBA) linker on the TiO_2 NP surface having the same

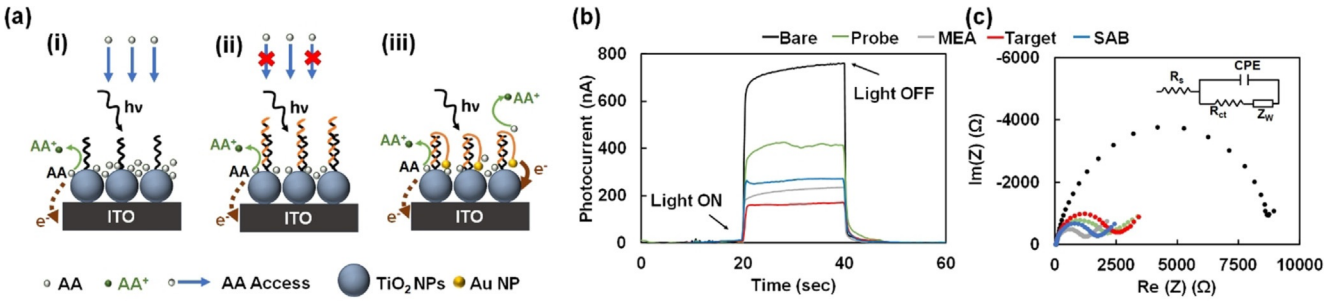

Figure 2. Photoelectrochemical signal generation on the differential DNA biosensor. a) Schematics showing the mechanism for photocurrent generation: (i) Bare TiO_2 electrode, (ii) after hybridization with complementary target, (iii) after hybridization with SAB. b) Photocurrent measurement after each step of the biosensor operation with 1 pM target in buffer using a 405 nm LED as excitation source at 160 $W m^{-2}$. All photocurrent measurements were performed at 0 V bias vs. Ag/AgCl. using 0.1 M ascorbic acid (AA) in 0.1 M PBS as electrolyte at each step of the biosensor construction. c) Electrochemical impedance spectroscopy measurements were performed in dark at open circuit potential vs. Ag/AgCl reference electrode using 2 mM $[Fe(CN)_6]^{3-/4-}$ in 0.1 M PBS and 0.1 M KCl as electrolyte. The equivalent circuit based on the shape of the Nyquist diagram is shown in the inset. Charge transfer resistance between the redox couple and the electrode is denoted by R_{ct}, which can be determined from the diameter of the semicircle. R_s, Z_w and CPE denote the solution resistance, Warburg impedance and constant phase element, respectively.

linker chemistry as dopamine, thereby enhancing the probability of quantum tunneling. It has also been hypothesized that DNA functionalization reduces carrier trapping sites by passivating the semiconductor (TiO_2) surface, thereby reducing charge recombination.[47] In order to further validate this finding, we performed a study by performing cyclic voltammetry (CV) in 0.1 M phosphate buffer (PBS) to show changes in charge transfer kinetics (Supporting Figure S3). This study showed that the amount of stored charges in the photoelectrodes were increased from 0.59 mC to 0.72 mC after DNA functionalization, indicating longer lived excitons. Similarly, the addition of MEA as a surface blocker further decreased the charge transfer resistance by 43%. Upon the hybridization of target DNA, the R_{ct} increased by 110%, which is attributed to increased steric hindrance between the redox species in the solution and the surface of the photoelectrode.[48] Introduction of the SAB resulted in a 33% decrease in R_{ct}, which is attributed to improved charge transfer kinetics due to the addition of Au NPs into the electrode film.[49,50]

To assess the ability of the differential PEC biosensor in analyzing DNA targets, we analyzed unlabeled DNA targets within a concentration range of 1 fM to 100 pM. As expected, when a solution containing target DNA was introduced to the device, the electrodes showed a PEC current that monotonically decreased with increasing target concentration (Figure 3a). As the concentration of target DNA in the first hybridization step decreases, there is a larger population of residual unhybridized probes, allowing more SAB strands to bind to the photoelectrode yielding a signal increase. As expected, this signal increase is larger at lower target DNA concentrations (Figure 3a,b (i)).

The differential PEC sensing strategy is then developed by combining the photocurrent change after target and SAB binding steps. More specifically, the absolute value of photocurrent decreases after the target hybridization was subtracted from the absolute value of photocurrent enhancement after SAB binding. The differential signal for each concentration was plotted to generate a calibration curve (Figure 3b). A linear fit to the calibration curve yielded a sensitivity of 49%/ $\log_{10}$M and LOD of 3 fM in buffer. The reverse signal-to-concentration effect observed here, where the largest signals are obtained at the lowest concentrations, allows high signal-to-noise ratios to be obtained at low concentrations that are often needed for clinical analysis, a feature that is not possible with traditional sandwich assays. This increase in signal at lower concentrations comes with the inherent drawback of differential signal processing: the experimental errors obtained from each measurement accumulate in the differential signal, leading to a loss of precision at all concentrations. Additionally, the use of two hybridization steps increases the overall assay time; however, preliminary experiments demonstrate that it may be possible to reduce the duration of each hybridization step (Supporting Figure S4).

In order to assess the applicability of the differential biosensor in analyzing DNA targets in complex biological matrices, we spiked target DNA at various concentrations into healthy patient urine (Figures 3c,d). The differential assay yielded a sensitivity of 25%/ $\log_{10}$M and LOD of 5 fM in urine. Both LOD and sensitivity deteriorate moderately in urine compared to buffer (less than a factor of two). This can be attributed to the biofouling of the photo electrode caused by the biological components present in urine.[51]

Adding the signal amplification step using the SAB significantly enhances the LOD of the system in both buffer (from 11 fM to 3 fM) and urine (from 73 fM to 5 fM) compared to using a single target binding step (Supporting Figure S5). The large enhancement in LOD ($\approx$15 times) observed in urine indicates that the differential signaling strategy is particularly important for compensating for the performance loss that is observed in complex biological samples. In addition to LOD, the differential strategy enhanced the assay sensitivity by about three times compared to the single binding assay for both buffer and urine samples. We further challenged the bioassay by spiking 1 pM of target DNA into human blood plasma (Supporting Figure S6). It should be noted that the bioassay utilized polyethylene glycol (PEG), in place of MEA, to reduce non-specific adsorption at the biosensor surface. The photocurrent changes observed after incubating the sensor with the target and SAB strands were similar to when human urine was used, indicating the potential use of this assay for biomarker detection in blood plasma.

To assess the specificity of the nucleic acid biosensor and its ability in distinguishing between fully matched and mismatched targets presenting point mutations, detection was carried out for targets with sequences presenting 1-base, 2-base and 3-base mismatches with the original sequences. The photocurrent changes obtained following each hybridization stage (after target and SAB binding) were then evaluated against those obtained for a perfectly complementary and a fully mismatched sequence tested in the same manner (Figure 4).

Following target binding, the current deceased by 48 ± 6%, 16 ± 4%, 14 ± 9%, and 6 ± 3% for matched, 1-base mismatched, 2-base mismatched, and non-complementary (NC) sequences, respectively (Figure 4a). This trend is largely attributed to the varying hybridization efficiency in each scenario, with fewer base mismatches resulting in more efficient target binding.[52,53] The matched, 1-base mismatched, 2-base mismatched, and NC sequences exhibited a 109 ± 6%, 160 ± 9%, 179 ± 8%, and 202 ± 4% increase in signal magnitude, respectively, following SAB binding (Figure 4a). In the case of the mismatched sequences, albeit inefficient, a fraction of the target sequences binds to available probe sites, still decreasing the available binding sites for SAB binding, which in turn reduces the SAB-induced signal enhancement. The differential signal enables highly distinguishable signal footprints to be realized for the different sequences with 60%, 123%, 163%, and 201% signal changes measured for matched, 1-base mismatched, 2-base mismatched, and NC sequences (Figure 4b). A statistical t-test was performed to assess the ability of the assays using one or two binding steps in distinguishing between different degrees of probe/target complementarity. Using differential signaling, we were able to distinguish between matched, 1-base mismatched, 2-base mismatched, and NC sequences

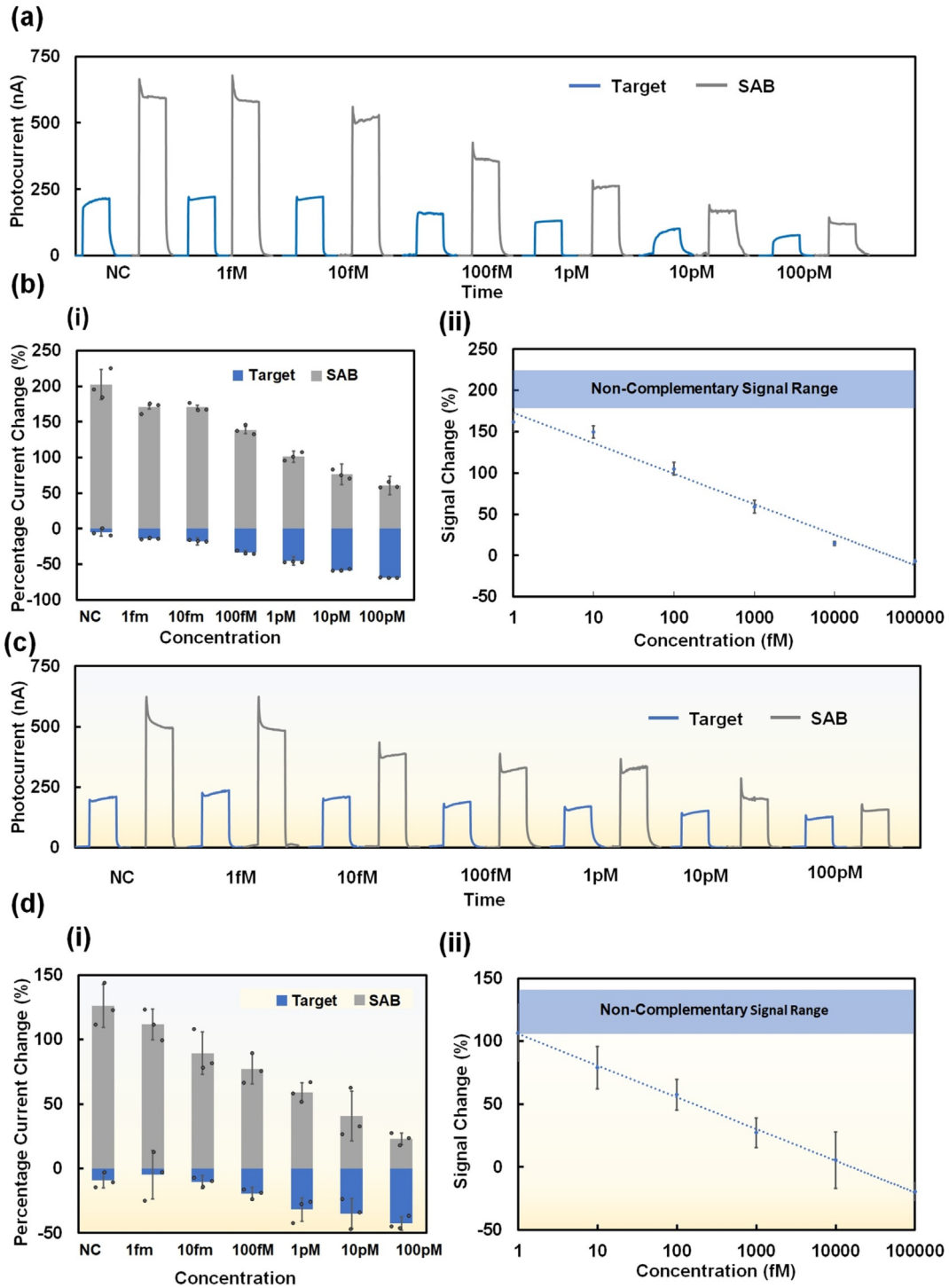

Figure 3. Limit of detection and sensitivity of the differential assay. All photocurrent measurements were performed at 0 V versus Ag/AgCl in 0.1 M ascorbic acid in 0.1 M PBS as electrolyte, illuminated using a 405 nm LED excitation source at 160 $W m^{-2}$. a,c) PEC graphs demonstrate signal responses following target and SAB binding in PBS and urine, respectively. b,d) Jitter plots (i) demonstrating the signal changes obtained from target and SAB binding in buffer and urine, respectively, obtained from (a) and (c). Representation of the differential signal (ii) obtained from the data presented in (i). The linear region of the calibration curve of the PBS graph was fitted using the equation $\Delta I\ \% = -49 \log_{10} C + 173$ (correlation coefficient of 97.97%) while the equation $\Delta I\ \% = -25 \log_{10} C + 106$ (correlation coefficient of 99.84%) was used to fit the urine data. This graph is depicted using a semi-log format, with the *x*-axis representing the logarithmic concentration ($\log_{10}$ M) of the target analyte.

(Figure 4b). On the contrary, the single target binding event can only distinguish matched from the 1-base mismatched sequence. The differential approach achieves a superior mismatch specificity with a high confidence level ($p < 0.05$ for all scenarios) as compared to its *signal-off* analogue.

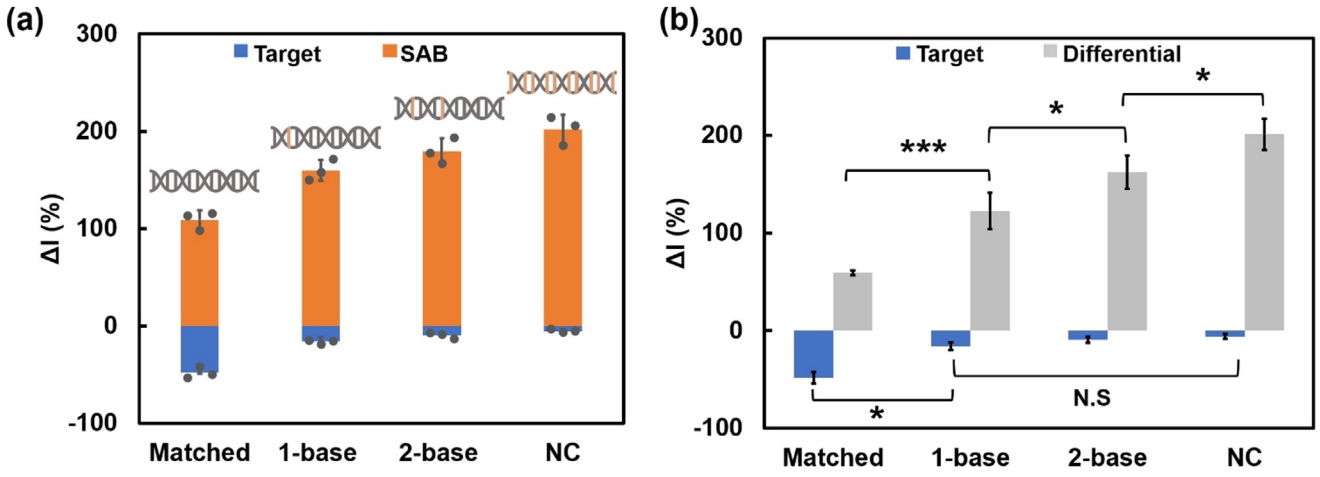

Figure 4. Specificity of the differential assay. a) Change in PEC current following hybridization with 1 pM of matched, 1-base mismatched, 2-base mismatched, and NC targets and SAB binding measured in 0.1 M PBS with 0.1 M AA. b) Differential and signal-off responses for the target sequences in (a) with * and *** representing $p < 0.05$ and $p < 0.001$, respectively.

We further assessed the static and dynamic stability of the differential PEC biosensor. PEC measurements of the electrodes stored under static conditions over a 7-day period following probe deposition (Supporting Figure S7a) revealed a small decrease in biosensor photocurrent (8% decrease from day 1 to day 7). Furthermore, the stability of the photoelectrodes under dynamic conditions, multiple light excitation and potential application, was assessed for 15 measurement cycles within a period of 800 s (Supporting Figure S7b), indicating stable photocurrents with a relative standard deviation of 6%.

Conclusion

In this work, we demonstrate a differential PEC assay using two subsequent and correlated hybridization events, first with an unlabeled target and then with a single amplification barcode tapping into the interaction of plasmatic and semiconductive nanoparticles, to detect unlabeled target DNA in both buffer and urine. The differential strategy exhibited a LOD of 3 fM in buffer and 5 fM in diluted urine, demonstrating significant improvement over a conventional signal-off strategy that used a single binding event (11 fM in buffer and 72 fM in urine) respectively. In addition to LOD, this assay enhanced the analytical sensitivity by a factor of three compared to an analogous assay that did not use differential signaling. The differential assay also demonstrated the ability to distinguish between sequences that were matched or contained 1- or 2-base mismatches with the detection probe, which was not possible using the non-differential approach. This work offers a new strategy for enhancing the limit-of-detection, sensitivity, and specificity of PEC biosensors, performance metrics that are key to the use of PEC biosensors in clinical decision making. The assay presented here, in terms of target length (25-mer) and concentration range (1 fM–100 pM), is ideally-suited for the analysis of short nucleic acid strands such as microRNA or DNA barcodes released from DNA machines such as DNAzymes,[54] CRISPR-Cas systems,[55] and strand displacement-based systems.[56]

Acknowledgements

This work was supported by NSERC, the Ontario Early Researcher Award granted to L.S., and a salary awarded to L.S. from the Canada Research Chairs Program. The electron microscopy was carried out at the Canadian Centre for Electron Microscopy (CCEM), a national facility supported by the NSERC and McMaster University. A.V and S.S. are recipients of the NSERC doctoral scholarships.

Conflict of interest

The authors declare no conflict of interest.

Keywords: biosensors · differential signaling · DNA barcodes · nucleic acid detection · photoelectrochemistry

[1] A. Victorious, S. Saha, R. Pandey, T. F. Didar, L. Soleymani, *Front. Chem.* **2019**, *7*, 617.
[2] B. Wang, J.-T. Cao, Y.-M. Liu, *Analyst* **2020**, *145*, 1121–1128.
[3] N. Zhang, L. Zhang, Y.-F. Ruan, W.-W. Zhao, J.-J. Xu, H.-Y. Chen, *Biosens. Bioelectron.* **2017**, *94*, 207–218.
[4] Z. Qiu, D. Tang, *J. Mater. Chem. B* **2020**, *8*, 2541–2561.
[5] X. Shen, D. Liu, C. Zhu, Y. Li, Y. Liu, T. You, *Electrochem. Commun.* **2020**, *110*, 106637.
[6] W.-W. Zhao, J.-J. Xu, H.-Y. Chen, *Biosens. Bioelectron.* **2017**, *92*, 294–304.
[7] W.-W. Zhao, J.-J. Xu, H.-Y. Chen, *Chem. Soc. Rev.* **2015**, *44*, 729–741.
[8] Y.-N. Zheng, W.-B. Liang, C.-Y. Xiong, Y. Zhuo, Y.-Q. Chai, R. Yuan, *Anal. Chem.* **2017**, *89*, 9445–9451.
[9] N. Hao, R. Hua, K. Zhang, J. Lu, K. Wang, *Anal. Chem.* **2018**, *90*, 13207–13211.
[10] Q. Hao, X. Shan, J. Lei, Y. Zang, Q. Yang, H. Ju, *Chem. Sci.* **2016**, *7*, 774–780.

[11] Y. Zhang, N. Hao, Z. Zhou, R. Hua, J. Qian, Q. Liu, H. Li, K. Wang, *Chem. Commun.* **2017**, *53*, 5810 – 5813.
[12] R. Hua, N. Hao, J. Lu, J. Qian, Q. Liu, H. Li, K. Wang, *Biosens. Bioelectron.* **2018**, *106*, 57 – 63.
[13] Q. Shen, L. Han, G. Fan, E. S. Abdel-Halim, L. Jiang, J.-J. Zhu, *Biosens. Bioelectron.* **2015**, *64*, 449 – 455.
[14] N. Hao, R. Hua, S. Chen, Y. Zhang, Z. Zhou, J. Qian, Q. Liu, K. Wang, *Biosens. Bioelectron.* **2018**, *101*, 14 – 20.
[15] M. Wang, H. Yin, Y. Zhou, C. Sui, Y. Wang, X. Meng, G. I. N. Waterhouse, S. Ai, *Biosens. Bioelectron.* **2019**, *128*, 137 – 143.
[16] P. Da, W. Li, X. Lin, Y. Wang, J. Tang, G. Zheng, *Anal. Chem.* **2014**, *86*, 6633 – 6639.
[17] L. Guo, Z. Li, K. Marcus, S. Navarro, K. Liang, L. Zhou, P. D. Mani, S. J. Florczyk, K. R. Coffey, N. Orlovskaya, Y.-H. Sohn, Y. Yang, *ACS Sens.* **2017**, *2*, 621 – 625.
[18] S. Saha, A. Victorious, R. Pandey, A. Clifford, I. Zhitomirsky, L. Soleymani, *ACS Appl. Mater. Interfaces* **2020**, *12*, 36895 – 36905.
[19] J. Shu, D. Tang, *Anal. Chem.* **2020**, *92*, 363 – 377.
[20] X.-P. Liu, J.-S. Chen, C. Mao, H.-L. Niu, J.-M. Song, B.-K. Jin, *Biosens. Bioelectron.* **2018**, *116*, 23 – 29.
[21] M. Zhao, G. C. Fan, J. J. Chen, J. J. Shi, J. J. Zhu, *Anal. Chem.* **2015**, *87*, 12340 – 12347.
[22] Z. Yan, Z. Wang, Z. Miao, Y. Liu, *Anal. Chem.* **2016**, *88*, 922 – 929.
[23] Y.-L. Huang, W. S. Chang, C. N. Van, H.-J. Liu, K.-A. Tsai, J.-W. Chen, H.-H. Kuo, W.-Y. Tzeng, Y.-C. Chen, C.-L. Wu, C.-W. Luo, Y.-J. Hsu, Y.-H. Chu, *Nanoscale* **2016**, *8*, 15795 – 15801.
[24] S. K. Cushing, J. Li, J. Bright, B. T. Yost, P. Zheng, A. D. Bristow, N. Wu, *J. Phys. Chem. C* **2015**, *119*, 16239 – 16244.
[25] A. Anne, C. Demaille, *J. Am. Chem. Soc.* **2008**, *130*, 9812 – 9823.
[26] C. Rivetti, C. Walker, C. Bustamante, *J. Mol. Biol.* **1998**, *280*, 41 – 59.
[27] S. Tan, A. Argondizzo, J. Ren, L. Liu, J. Zhao, H. Petek, *Nat. Photonics* **2017**, *11*, 806 – 812.
[28] C. Clavero, *Nat. Photonics* **2014**, *8*, 95.
[29] L. P. Reynaldo, A. V. Vologodskii, B. P. Neri, V. I. Lyamichev, *J. Mol. Biol.* **2000**, *297*, 511 – 520.
[30] B. A. Baker, V. T. Milam, *Nucleic Acids Res.* **2011**, *39*, e99 – e99.
[31] J. C. Traeger, D. K. Schwartz, *Langmuir* **2017**, *33*, 12651 – 12659.
[32] N. R. Sundah, N. R. Y. Ho, G. S. Lim, A. Natalia, X. Ding, Y. Liu, J. E. Seet, C. W. Chan, T. P. Loh, H. Shao, *Nat. Biomed. Eng.* **2019**, *3*, 684 – 694.
[33] H. Schwarzenbach, D. S. B. Hoon, K. Pantel, *Nat. Rev. Cancer* **2011**, *11*, 426 – 437.
[34] J. Hayes, P. P. Peruzzi, S. Lawler, *Trends Mol. Med.* **2014**, *20*, 460 – 469.
[35] S. Zhou, J. Jin, J. Wang, Z. Zhang, J. H. Freedman, Y. Zheng, L. Cai, *Acta Pharmacol. Sin.* **2018**, *39*, 1073 – 1084.
[36] L. Tribolet, E. Kerr, C. Cowled, A. G. D. Bean, C. R. Stewart, M. Dearnley, R. J. Farr, *Front. Microbiol.* **2020**, *11*, 1197.
[37] S. Saha, Y. Chan, L. Soleymani, *ACS Appl. Mater. Interfaces* **2018**, *10*, 31178 – 31185.
[38] H. Choi, W. T. Chen, P. V. Kamat, *ACS Nano* **2012**, *6*, 4418 – 4427.
[39] J. Li, S. K. Cushing, D. Chu, P. Zheng, J. Bright, C. Castle, A. Manivannan, N. Wu, *J. Mater. Res.* **2016**, *31*, 1608 – 1615.
[40] R. Sundararaman, P. Narang, A. S. Jermyn, W. A. Goddard, H. A. Atwater, *Nat. Commun.* **2014**, *5*, 5788.
[41] T. Barman, A. A. Hussain, B. Sharma, A. R. Pal, *Sci. Rep.* **2015**, *5*, 18276.
[42] M. L. Brongersma, N. J. Halas, P. Nordlander, *Nat. Nanotechnol.* **2015**, *10*, 25.
[43] C. L. Manzanares-Palenzuela, E. G. R. Fernandes, M. J. Lobo-Castañón, B. López-Ruiz, V. Zucolotto, *Electrochim. Acta* **2016**, *221*, 86 – 95.
[44] W. Tu, H. Cao, L. Zhang, J. Bao, X. Liu, Z. Dai, *Anal. Chem.* **2016**, *88*, 10459 – 10465.
[45] Y. Ju, X. Hu, Y. Zang, R. Cao, H. Xue, *Anal. Methods* **2019**, *11*, 2163 – 2169.
[46] R. Imani, M. Pazoki, A. Tiwari, G. Boschloo, A. P. F. Turner, V. Kralj-Iglič, A. Iglič, *Nanoscale* **2015**, *7*, 10438 – 10448.
[47] Ö. Ateş Sönmezoğlu, S. Akın, B. Terzi, S. Mutlu, S. Sönmezoğlu, *Adv. Funct. Mater.* **2016**, *26*, 8776 – 8783.
[48] Y. Chu, R. Wu, G.-C. Fan, A.-P. Deng, J.-J. Zhu, *ACS Sustainable Chem. Eng.* **2018**, *6*, 11633 – 11641.
[49] S. P. Lim, A. Pandikumar, N. M. Huang, H. N. Lim, *RSC Adv.* **2015**, *5*, 44398 – 44407.
[50] J.-M. Li, C.-W. Tsao, M.-J. Fang, C.-C. Chen, C.-W. Liu, Y.-J. Hsu, *ACS Appl. Nano Mater.* **2018**, *1*, 6843 – 6853.
[51] M. A. Johansson, K.-E. Hellenäs, *Analyst* **2004**, *129*, 438 – 442.
[52] L. Zhang, Y. Sun, Y.-Y. Liang, J.-P. He, W.-W. Zhao, J.-J. Xu, H.-Y. Chen, *Biosens. Bioelectron.* **2016**, *85*, 930 – 934.
[53] Y. Jin, X. Yao, Q. Liu, J. Li, *Biosens. Bioelectron.* **2007**, *22*, 1126 – 1130.
[54] Y. Zhao, L. Zhou, Z. Tang, *Nat. Commun.* **2013**, *4*, 1493.
[55] R. Bruch, J. Baaske, C. Chatelle, M. Meirich, S. Madlener, W. Weber, C. Dincer, G. A. Urban, *Adv. Mater.* **2019**, *31*, 1970365.
[56] P. Miao, T. Zhang, J. Xu, Y. Tang, *Anal. Chem.* **2018**, *90*, 11154 – 11160.

Manuscript received: October 26, 2020
Revised manuscript received: December 16, 2020
Accepted manuscript online: January 5, 2021
Version of record online: February 17, 2021

